

Energy-Aware Dynamic Planning Algorithm for Autonomous UAVs

Adam Seewald¹, Hector Garcia de Marina², and Ulrik Pagh Schultz¹

Abstract—abstract
abstract
abstract
abstract
abstract
abstract
abstract
abstract
abstract
abstract
abstract
abstract
abstract

I. INTRODUCTION

Many scenarios involving unmanned aerial vehicles (UAVs), such as precision agriculture, search and rescue, and surveillance, require high autonomy but have limited energy budgets. A typical example of these scenarios is a UAV following a path and performing some on-board computational tasks. For instance, the UAV might detect ground patterns and notify other ground-based actors with little human interaction. We refer to such computational tasks that can be dynamically replanned and adapted as *computations*. We are interested in the energy optimization of the path and computations under uncertainty (atmospheric interferences) and refer to it as energy-aware dynamic planning. Such planning would find optimal tradeoffs between the path, computations, and energy requirements. Current generic planning solutions for outdoor UAVs do not plan the path and computations dynamically, nor are they energy-aware. They are often semi-autonomous: the path and computations are static and usually defined using planning software [1] (for instance [2] and [3]). Such a state of practice has prompted us to propose an *energy-aware dynamic planning algorithm* for UAVs. The algorithm combines and generalizes some of the past body of knowledge on mobile robot planning problems and addresses the increasing *computational demands* and their relation to

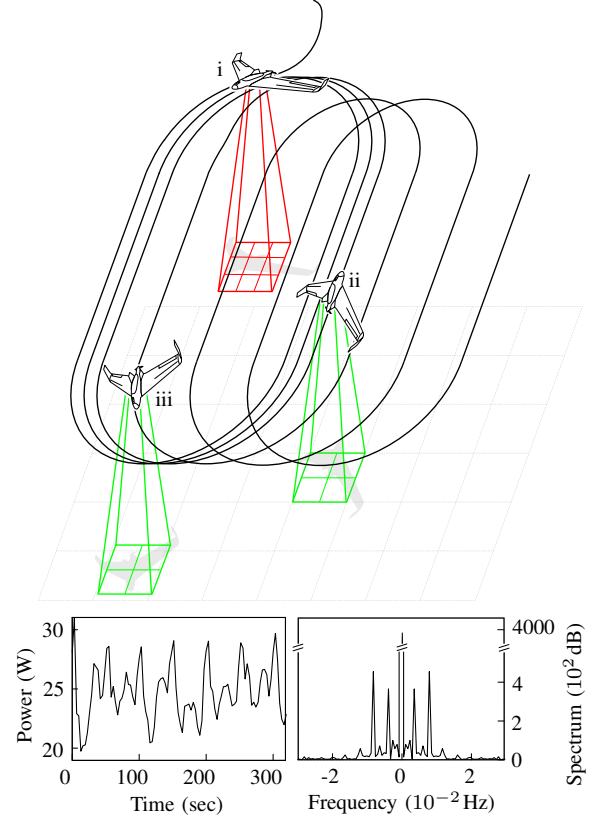


Fig. 1. An initial plan of an agricultural scenario replanned dynamically in terms of the path and computations all together. An initial plan (in i) is adapted computation-wise (in ii) and path-wise (in iii). In the bottom left, the collected energy data of a physical UAV (Opterra fixed-wing drone) flying the scenario, along the power spectrum on the right.

energy consumption, path, and autonomy for the UAV planning problem.

Planning algorithms literature for mobile robots includes topics such as trajectory generation and path planning. Generally, the algorithms select an energy-optimized trajectory [4], e.g., by maximizing the operational time [5]. However, they apply to a small number of robots [6] and focus exclusively on planning the trajectory [7], despite compelling evidence for the energy consumption also being significantly influenced by computations [8]. Given the availability of powerful GPU-equipped mobile hardware [9], the use of computations is expected to increase in the near future [10]–[12]. More complex planning, which includes a broader concept of

This work is supported and partly funded by the European Union's Horizon2020 research and innovation program under grant agreement No. 779882 (TeamPlay).

¹Adam Seewald, Ulrik Pagh Schultz are with the SDU UAS Center, Mærsk Mc-Kinney Møller Institute, University of Southern Denmark, Odense, Denmark. Email: ads@mmi.sdu.dk.

²Hector Garcia de Marina is with the Faculty of Physics, Department of Computer Architecture and Automatic Control, Universidad Computense de Madrid, Spain.

the plan being a set of tasks and a path, all focus on the trajectory [8], [13] and apply to a small number of robots [14], [15]. For UAVs specifically, rotorcrafts have also gained interest in terms of algorithms for energy-optimized trajectory generation [16], [17].

Unlike most of the past planning algorithms literature, our algorithm plans the path and computations all together. To model the path we use multiple mathematical functions. In Figure 1, the path contains multiple circles and lines. To model the computations we use *powprofiler*, a profiling tool presented in previous work [18]. To guide the UAV we use a vector field [19] that converges smoothly to the path. The use of vector fields for guidance is indeed widely discussed in the literature [19]–[24].

To achieve the energy-aware dynamic planning, we further introduce and formally proof a periodic energy model that accounts for the uncertainty. We use Fourier analysis to derive the model, and state estimation to address the uncertainty. Periodicity is often present due to repetitive patterns in the plan [25]. Indeed, UAV scenarios often iterate over a set of tasks and paths (e.g., monitoring or search and rescue). Given that the plan is periodic, we expect the energy consumption to approximately evolve periodically. In Figure 1, some collected energy data from a UAV flying a survey scenario along its power spectrum motivates our choice.

In the spirit of reducing costs and resources, we showcase the algorithm using the problem of dynamic planning for a precision agriculture fixed-wing UAV. Precision agriculture is often put into practice [26] with ground mobile robots used for harvesting [27]–[32], and UAVs for preventing damage and ensuring better crop quality [1], [33]. The plan is structured as follows. Path-wise, the UAV flies in circles and lines covering a polygon. Computation-wise, it detects obstacles using a convolutional neural network (CNN) and notifies grounded mobile robots employed for harvesting. The algorithm alters the plan; it controls the processing rate and the radius of the circles (affecting the distance between the lines). Figure 1 shows such plan. We observe that not only the path but also the computations significantly impact the energy, with a potential extension of up to 13 minutes over an hour by switching from the highest to the lowest level of computations in presence of a standard battery (see Section V).

The remainder of the paper is organized as follows. The overview of dynamic planning, some preliminaries, and problem definition are provided in Section II. We show a suitable model for the energy in Section III, and propose the algorithm in Section IV. In Section V, we present the results and showcases the performances. We then derive some conclusions in Section VI. Finally, we provide some additional information in Appendixes.

II. PLANNING OVERVIEW

The algorithm inputs a user-specified initial plan that consist of different stages. At each stage the plan contains some parameters that allow to alter the path and computations along an energy budget. The alterations are bounded. There is one path constraint set which bounds the path and multiple computation constraint sets, one per each computation parameter, that bound computations. In Figure 1, there are two parameters. One relative to the path (ii has a shorter distance between the lines than iii), and the other one to the computations (i processes more images per second than ii).

The algorithm outputs the control (the parameters) using output model predictive control (MPC) [34] where it checks the satisfaction of the battery constraints. The control is data-driven. Energy sensor data estimates some coefficients of an energy model used to predict future energy consumption in presence of uncertainty. The energy budget is the battery capacity and other battery parameters. These are fixed values that are not replanned by the algorithm. Our goal is to complete the plan with the highest possible parameters as the UAV flies and its batteries drain.

A. Plan definition

Let us adopt the following mathematical notation. Given an integer a , $[a]$ is the set $\{0, 1, \dots, a\}$, $[a]^+$ the set $[a]/\{0\}$. Bold lower-case letters indicates vectors. $c_{i,j}$ the j -th parameter of the i -th parameters set c_i . $\underline{c}_{i,j}, \bar{c}_{i,j}$ are the lower and upper bounds of the parameter $c_{i,j}$. The set $\langle c_{i,1}, c_{i,2}, \dots, c_{i,n} \rangle$ is an ordered list $\langle c_i \rangle$ of n parameters.

Let us assume that the path at stage i can be altered with ρ path parameters $\mathcal{C}_i^\rho := \{c_{i,1}, c_{i,2}, \dots, c_{i,\rho}\}$, and the computations with σ computations parameters $\mathcal{C}_i^\sigma := \{c_{i,\rho+1}, c_{i,\rho+2}, \dots, c_{i,\rho+\sigma}\}$. We then express the path as a continuous twice differentiable function $\varphi_i : \mathbb{R}^2 \times \mathbb{R}^\rho \rightarrow \mathbb{R}$ of a point and the path parameters. The function returns a metric of the distance between the point and the nominal trajectory. We express the computations as the value of the computations parameters. We discuss the concrete meaning of the value of path parameters in Subsection III-A, and computations parameters in Subsection III-B.

Definition II.1 (Stage, plan, triggering, and final point). The i -th stage Γ_i at time instant k of a plan Γ is defined as the ordered list

$$\begin{aligned} \Gamma_i := & \{ \langle \varphi_i(\mathbf{p}_k, c_{i,1}, \dots, c_{i,\rho}), c_{i,\rho+1}, \dots, c_{i,\rho+\sigma} \rangle \\ & | \exists \mathbf{p}_k, \varphi_i(\mathbf{p}_k, c_{i,1}, \dots, c_{i,\rho}) \in \mathcal{C}_i, \\ & \forall j \in [\sigma]^+, c_{i,\rho+j} \in \mathcal{S}_{i,j} \}, \end{aligned}$$

where $\mathcal{C}_i := [\underline{c}_i, \bar{c}_i] \subseteq \mathbb{R}$ is the path constraint set, and $\mathcal{S}_{i,j} := [\underline{c}_{i,\rho+j}, \bar{c}_{i,\rho+j}] \subseteq \mathbb{Z}_{\geq 0}$ the j -th computation

of the column vectors. We note that there is a limited number (two) of linear combinations of the column vectors being these linearly dependent (from \implies). ■

The proposition is a necessary (\Leftarrow) and sufficient (\Rightarrow) condition for periodicity. The algorithm finds n initializing it to one and finding the value which satisfies the proposition. It then measures the time between the stages and assumes the initial period is one. The periods might be different for different j s due to atmospheric interferences.

Problem II.1 (UAV planning problem). Consider an initial plan Γ from Definition II.1 that satisfies Assumption II.1. We are interested in the planning of the parameters c_i , $\forall i \in [l]^+$ and in the guidance to the path resulting from such plan for the UAV planning problem.

III. PERIODIC ENERGY MODEL

We refer to the instantaneous energy consumption evolution simply as the energy signal. We model the energy using energy coefficients $\mathbf{q} \in \mathbb{R}^m$ that characterize such energy signal. The coefficients are derived from Fourier analysis (the size of the energy coefficients vector m is related to the order of a Fourier series) and estimated using a state estimator.

We proof a relation between the energy signal and the energy coefficients in Lemma III.1. We show after the main results how this approach allows us variability in terms of the systems behaving periodically, piece-wise periodically, or merely linearly with sporadic periodicity.

Once we illustrate the energy model, we enhance it with the energy contribution of the path in Subsection III-A, and of the computations in Subsection III-B.

Let us consider a periodic energy signal of period T , and a Fourier series of an arbitrary order $r \in \mathbb{Z}_{\geq 0}$ for the purpose of modeling of the energy signal

$$h(t) = a_0/T + (2/T) \sum_{j=1}^r (a_j \cos \omega j t + b_j \sin \omega j t), \quad (1)$$

where $h : \mathbb{R}_{\geq 0} \rightarrow \mathbb{R}$ maps time to the instantaneous energy consumption, $\omega := 2\pi/T$ is the angular frequency (T is the period from Definition II.2), and $a, b \in \mathbb{R}$ the Fourier series coefficients.

The energy signal can be modeled by Equation (1) and by the output of a linear model

$$\begin{aligned} \dot{\mathbf{q}} &= A\mathbf{q} + B\mathbf{u}, \\ y &= C\mathbf{q}, \end{aligned} \quad (2)$$

where $y \in \mathbb{R}$ is the instantaneous energy consumption.

The state \mathbf{q} contains the energy coefficients

$$\begin{aligned} \mathbf{q} &= [\alpha_0 \quad \alpha_1 \quad \beta_1 \quad \cdots \quad \alpha_r \quad \beta_r]^T, \\ A &= \begin{bmatrix} 0 & & & \\ & \ddots & & \\ & & A_r & \end{bmatrix}, A_j \begin{bmatrix} 0 & \omega j \\ -\omega j & 0 \end{bmatrix}, \\ C &= (1/T) [1 \quad 1 \quad 0 \quad \cdots \quad 1 \quad 0], \end{aligned} \quad (3)$$

where $\mathbf{q} \in \mathbb{R}^m$ with $m = 2r+1$, $A \in \mathbb{R}^{m \times m}$ is the state transmission matrix, and $C \in \mathbb{R}^m$ is the output matrix. In matrix A , the top left entry is zero, the diagonal entries are A_1, \dots, A_r , the remaining entries are zeros.

The linear model in Equation (2) allows us to include the control in the model of Equation (1).

Lemma III.1 (Signal, output equality). Suppose control \mathbf{u} is a zero vector, matrices A, C are described by Equation (3), and the initial guess \mathbf{q}_0 is

$$\mathbf{q}_0 = [a_0 \quad a_1/2 \quad b_1/2 \quad \cdots \quad a_r/2 \quad b_r/2]^T.$$

Then, the signal h in Equation (1) is equal to the output y in Equation (2).

Proof. The equality of the signal and output is achieved by a proper choice of the items of matrices A, C and the initial guess \mathbf{q}_0 . We refer the reader to Appendix I for a formal proof, where we justify the choices of the items of the matrices and of the initial guess. ■

Let us consider for practical reasons the discretized version of the system in Equation 2.

Let us suppose that at time instant k the plan reached the i -th stage Γ_i .

The control along with the input matrix

$$\begin{aligned} \mathbf{u}_k &= [c_{k,1} \quad \cdots \quad c_{k,\rho} \quad c_{k,\rho+1} \quad \cdots \quad c_{k,\rho+\sigma}]^T, \\ B &= \begin{bmatrix} 0 & \cdots & 0 & 1 & \cdots & 1 \end{bmatrix} \\ \mathbf{u} &:= \text{diag}(\nu_i)(\mathbf{u}_k - \mathbf{u}_{k-1}) - \tau_i, \end{aligned} \quad (4)$$

where $\mathbf{u} \in \mathbb{R}^n$ is the control with $n = \rho + \sigma$. Matrix $B \in \mathbb{R}^{m \times n}$ contains zeros except the first row where the first ρ columns are still zeros and the remaining σ are ones. $\nu_i = [\nu_{i,1} \quad \cdots \quad \nu_{i,\rho+\sigma}]^T$ and $\tau_i = [\tau_{i,1} \quad \cdots \quad \tau_{i,\rho+\sigma}]^T$ are scaling factors quantifying the contribution to the plan of a given parameter in terms of time (for the first ρ parameters) and the power (for the remaining σ).

We elucidate how we derive these factors in the next two subsections.

A. Path parameters energy contribution

Let us assume that the set

$$\mathcal{P}_i := \{\mathbf{p}_k \mid \varphi_i(\mathbf{p}_k, c_{i,1}, \dots, c_{i,\rho}) \in \mathcal{C}_i\}, \quad (5)$$

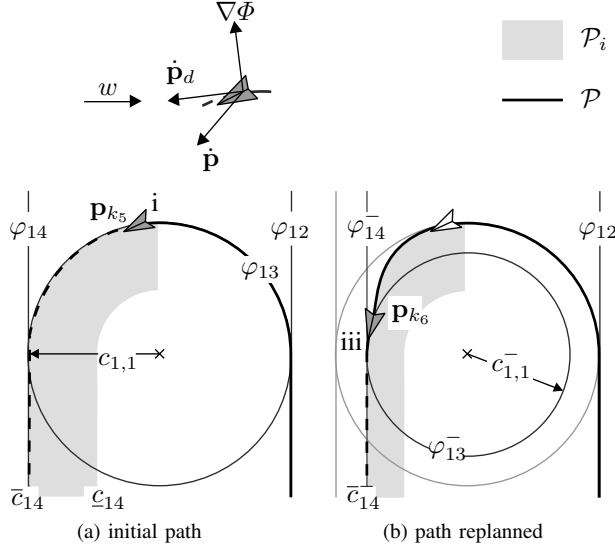


Fig. 4. The alteration of the path parameter $c_{1,1}$, the radius of the circle (it corresponds to the alteration of the path in Figure 1).

delimits the area where the i -th path φ_i is free to evolve using the path parameters $c_{i,1}, \dots, c_{i,\rho}$ (the gray area in Figure 4). φ_i is a function of the two coordinates and is equal to zero when a point \mathbf{p}_k is on the path. Physically, this means the UAV is flying exactly over the nominal trajectory. The path parameters allows to change the path. They are a way to alter the nominal trajectory in the initial plan and thus alter the energy by e.g., changing the flying time in the example in Figure 1. In fact, the algorithm uses the set from Equation (5) to find the path parameters such that φ_i has the highest energy consumption, while still respecting the energy budget. In Figure 4, the parameter radius of the circle $c_{1,1}$ is replanned as, e.g., adverse atmospheric conditions do not allow to terminate the plan.

We derive the new position \mathbf{p}_{k+1} computing the vector field $\nabla\varphi_i := [\partial\varphi_i/\partial x \ \partial\varphi_i/\partial y]^T$, and the direction to follow in the form of velocity vector [19]

$$\dot{\mathbf{p}}_d(\mathbf{p}_k) := E\nabla\varphi_i - k_e\varphi_i\nabla\varphi_i, \quad E = \begin{bmatrix} 0 & 1 \\ -1 & 0 \end{bmatrix}, \quad (6)$$

where E specifies the rotation (it influence the tracking direction), and $k_e \in \mathbb{R}_{\geq 0}$ the gain to adjusts the speed of convergence. The direction the velocity vector $\dot{\mathbf{p}}_d$ is pointing at is generally different from the course heading $\dot{\mathbf{p}}$ due to the atmospheric interferences (wind $w \in \mathbb{R}$ in the top of Figure 4).

The scaling factors for the path parameters from Equation (4) are derived empirically. For the example in Figure 4, we can obtain the scaling factor $\nu_{1,1}$ measuring the time needed to compute the path with the lowest configuration \underline{c}_1 , \underline{t} and the highest \bar{t} . The variation of the control hence results in an approximate measure of

the plans' time variation

$$\begin{aligned} \nu_{i,j} &= ((\bar{t} - \underline{t})/(\bar{c}_{i,j} - \underline{c}_{i,j}))/\rho, \\ \tau_{i,j} &= (\underline{c}_{i,j}(\underline{t} - \bar{t})/(\bar{c}_{i,j} - \underline{c}_{i,j}) + \underline{t})/\rho, \end{aligned} \quad (7)$$

$\forall j \in [\rho]^+$. Moreover, let $\nu_{i,1}, \dots, \nu_{i,\rho}$ be zero when the parameters set $c_i^\rho = \{\emptyset\}$.

B. Computations parameters energy contribution

Let us recall from Definition II.1 that the i -th stage Γ_i of the plan Γ contains the computations parameters which characterize the computations. We assess the energy cost of these computations using `powprofiler`, the open-source modeling tool adapted from earlier work on computational energy analysis [18], [35], and energy estimation of a fixed-wing UAV [25].

For this purpose, we assume the UAV carries an embedded board that runs the computations. The tool measures the instantaneous energy consumption of a subset of possible computations parameters within the computation constraint sets and builds an energy model: a linear interpolation, one per each computation.

The computations are implemented by software components, e.g., ROS nodes in a ROS based system. The user implements these nodes such that they change the computational load with node-specific ROS parameters, the computations parameters. In a generic software component system, the user maps the computational load to the arguments. In both cases, with ROS [36] or with generic software components system [35], the tool performs automatic modeling. For instance, if the computation is a CNN object detector, the computation parameter $c_{i,\rho+1}$ might correspond to frames-per-second (fps) rate. The tool then changes the detection frequency.

We note that while the path can differ for each stage, the tasks remain the same. However, the user can inhibit or enable a computation varying its computation constraint set.

Let us define $g : \mathbb{Z}_{\geq 0} \rightarrow \mathbb{R}_{\geq 0}$ as the instantaneous computational energy consumption value obtained using the tool.

The scaling factors that quantifies the energy contribution of the computations parameters are derived similarly to Equation (7)

$$\begin{aligned} \nu_{i,j} &= (g(\bar{c}_{i,j}) - g(\underline{c}_{i,j})) / (\bar{c}_{i,j} - \underline{c}_{i,j}), \\ \tau_{i,j} &= \underline{c}_{i,j}(g(\underline{c}_{i,j}) - g(\bar{c}_{i,j})) / (\bar{c}_{i,j} - \underline{c}_{i,j}) + g(\underline{c}_{i,j}), \end{aligned}$$

$\forall j \in [\rho + 1, \rho + \sigma]$. Moreover, let $\nu_{i,\rho+1}, \dots, \nu_{i,\rho+\sigma}$ be zero when the parameters set $c_i^\sigma = \{\emptyset\}$.

The factors thus add the computational energy component to the model in Equation (2).

IV. ALGORITHM

The main purpose of the algorithm is to output a valid control sequence $\mathbf{u} := \{\mathbf{u}_0, \mathbf{u}_1, \dots\}$ at each time step given an initial plan Γ and to guide the UAV on a valid path: to solve Problem II.1.

Definition IV.1 (Valid control sequence and path). Given a close strictly positive discrete interval $\mathcal{J} := [j - n + 1, j]$ (for $j \in \mathbb{Z}_{>0}, j \leq l$ and n given in Assumption II.1), a *control sequence* \mathbf{u} is *valid* on \mathcal{J} if for every stage $\Gamma_{i-1}, i \in \mathcal{J}$ there exists a control \mathbf{u}_k that produce the next stage Γ_i .

The path \mathcal{P} resulting from such control sequence is a *valid path* on \mathcal{J}

$$\mathcal{P} := \{\mathbf{p}_k \mid \exists \mathbf{u}_k, \forall i \in \mathcal{J}, \langle \varphi_i(\mathbf{p}_k, c_k^\rho), c_k^\sigma \rangle \in \Gamma_i\},$$

where we recall that $\mathbf{u}_k = [c_k^\rho \ c_k^\sigma]^T$ from Equation (4).

Let us consider the assumption that at least one period in the user-defined initial plan is valid.

Assumption IV.1 (Period validity). Given an initial plan Γ , we assume that $\exists i \in [l/n]^+$ s.t. the period $\Gamma_{(i-1)n+1}, \dots, \Gamma_{in}$ is valid.

Let us proof that if the plan is periodic and one period is valid, then the plan is valid.

Theorem IV.2 (Valid periodic plan). Suppose Assumption IV.1, Lemma III.1, and Proposition II.1 hold (a period of the plan is valid, its energy evolution is described by Equation (2), and the plan is periodic). Then the plan is valid and its energy evolution modeled by the periodic energy model in Section III-A.

Proof. From Definition IV.1, Assumption IV.1, we know that there exists a $\mathcal{J} \subseteq [l]^+$ where the path is valid, and from Proposition II.2 we know that the path is periodic. Hence if the set \mathcal{J} is valid, then also the set $i[j - n + 1, j] \subseteq [l]^+$ is valid for a given i . From the assumption we note that $i \in [l/n]^+$ and, due to the proposition, $\mathcal{J} = [l]^+$. Due to the periodicity, Lemma III.1 allows us to use the proposed approach to model the energy. ■

We can thus output a valid control sequence for the initial plan Γ . For practical means, we consider some realistic constraints to the energy of a flying UAV. We illustrate such constraints in the following subsection.

A. Output and control constraint sets

We stated earlier the output y —the instantaneous energy consumption—evolves in $\mathbb{R}_{\geq 0}$. This is generally untrue. Physical UAVs are bounded by strict energy budgets due to battery limitations.

Algorithm Energy-Aware Dynamic Planning

```

1:  $\mathbf{p}_{k-1} \leftarrow \mathbf{p}_0, \mathbf{q}_{k-1} \leftarrow \mathbf{q}_0$ 
2:  $\mathbf{u}_{k-2}, \mathbf{u}_{k-1} \leftarrow \{\emptyset\}$ 
3: for  $i \in [l]^+$  do
4:   while  $\mathbf{p}_{k-1} \neq \mathbf{p}_{\Gamma_i}$  do
5:      $\mathbf{u}_k \leftarrow \arg \max_{\mathbf{u}} \sum_{j=k-1}^{k+N-2} l(\mathbf{q}_j, \mathbf{u}_j) + V_f(\mathbf{q}_{k+N-1})$ 
6:      $\hat{\mathbf{q}}_k \leftarrow A\mathbf{q}_{k-1} + B(\text{diag}(\nu_i)(\mathbf{u}_k - \mathbf{u}_{k-1}) - \tau_i)$ 
7:      $\mathbf{q}_k \leftarrow$  the estimate of the state from  $\hat{\mathbf{q}}_k$  and sensor data
8:      $\mathbf{p}_k \leftarrow \mathbf{p}_{k-1} + \dot{\mathbf{p}}_d(\mathbf{p}_{k-1})/v$ 
9:      $k \leftarrow k + 1$ 
10:   end while
11: end for
```

Let us hence consider the state of charge (SoC) b of a UAV battery with a simplistic difference equation [25]

$$b_k = b_{k-1} - k_b \left(V - \sqrt{V^2 - 4R_r y_k} \right) / (2R_r Q_c),$$

where k_b is the battery coefficient determined experimentally, $V \in \mathbb{R}$ is the internal battery voltage measured in volts, $R_r \in \mathbb{R}$ the resistance measured in ohms, and $Q_c \in \mathbb{R}$ the constant nominal capacity measured in amperes per hour.

Definition IV.2 (Output, control constrain sets). The output constrain set is then the set

$$\mathcal{Y}_k := \{y_k \mid y_k \in [0, b_k Q_c V] \subseteq \mathbb{R}_{\geq 0}\},$$

and $\max \mathcal{Y}_k$ is the maximum discharge capacity by the internal battery voltage—the maximum instantaneous energy consumption. b_{k-1} can be determined using a sensor.

The control constraint set is the path constraint set for the path parameters and computation constraint sets for the computation parameters (Definition II.1)

$$\mathcal{U}_k := \begin{cases} \mathcal{C}_i & \text{for } c_{i,j} \text{ with } j \leq \rho \\ \mathcal{S}_{i,j-\rho} & \text{for } c_{i,j} \text{ with } \rho < j \leq \sigma \end{cases}.$$

B. Deployment algorithm

The algorithm first initializes the position, energy coefficients, and control (line 2). It updates the position at line 8, using the expression from Equation (6) and the velocity $v \in \mathbb{R}_{\geq 0}$. The expression depends on the path φ_i from stage Γ_i . The algorithm iterates all the stages in the plan Γ (line 3), and enters the next stage Γ_{i+1} when the UAV reaches the triggering point \mathbf{p}_{Γ_i} (we recall the FSM in Definition II.1).

The energy coefficients are updated at line 6, using the expression from Equation (2). The a priori state estimate $\hat{\mathbf{q}}_k$ is refined using a state estimator—such as Kalman filter [37]—and the data from an energy sensor (line 7). At

line 5, the algorithm uses robust output feedback model predictive control (MPC) [34] to select the control \mathbf{u}_k for a given horizon $N \in \mathbb{Z}_{>0}$ from the cost function

$$\begin{aligned} V_f(\mathbf{q}_k) &:= (1/2)\mathbf{q}_k^T \text{diag}(C)\mathbf{q}_k, \\ l(\mathbf{q}_k, \mathbf{u}_k) &:= (1/2)(\mathbf{q}_k + B\mathbf{u})^T \text{diag}(C)(\mathbf{q}_k + B\mathbf{u}), \end{aligned} \quad (8)$$

where $\text{diag}(C)$ is a diagonal matrix with the items of C from Equation (3), and \mathbf{u} is defined in Equation (4).

We note from Lemma III.1 that the expression in Equation (8) denotes the square of the predicted power. Moreover, higher the horizon, higher the complexity and the robustness of the control to the output constraints.

We further note that at every step of the summary on line 5 the algorithm has to evolve the state to check if the output satisfies the output constraint set, and if the control satisfies the control constraint set. In particular, at each steps it performs the subrou-tine

```
while  $\bar{c}_i \notin \mathcal{U}_k, y_k \notin \mathcal{Y}_k$  do
   $\bar{c}_i \leftarrow \bar{c}_i - \delta$ 
end while
 $\mathbf{u}_k \leftarrow \bar{c}_i$ 
```

where $\delta \in \mathbb{R}^p \times \mathbb{Z}_{\geq 0}^\sigma$ are reduction steps (the maximum values of path and computational parameters are reduced by the steps if they don't meet the constraints). To evaluate the inclusion in the output control set, the algorithm evolves the state from its previous estimate similarly as at line 6.

We finally note that one can express the tradeoffs between parameters (e.g., a decrement in the distance between the lines in a survey scenario is related to a decrement in the number of detections per second) enriching the control constraint set with the constraints

$$R_i \mathbf{u}_k - r_i \geq 0,$$

where $r_i \in \mathbb{R}^n$ and $R_i \in \mathbb{R}^{n \times n}$ expresses the relation between the parameters (if R_i is the identity matrix, there is no relation between the parameters).

V. RESULTS

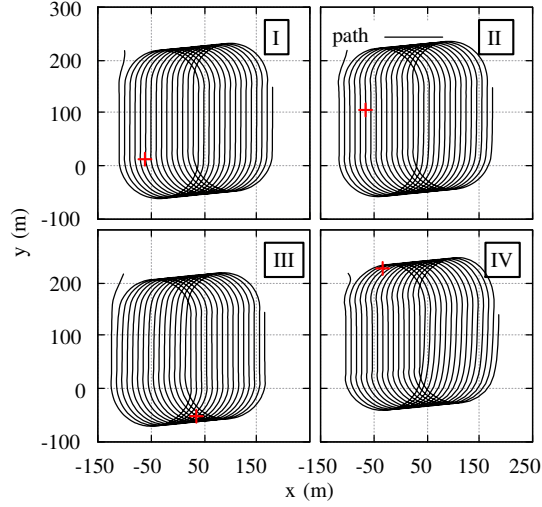
*

VI. CONCLUSION AND FUTURE WORK

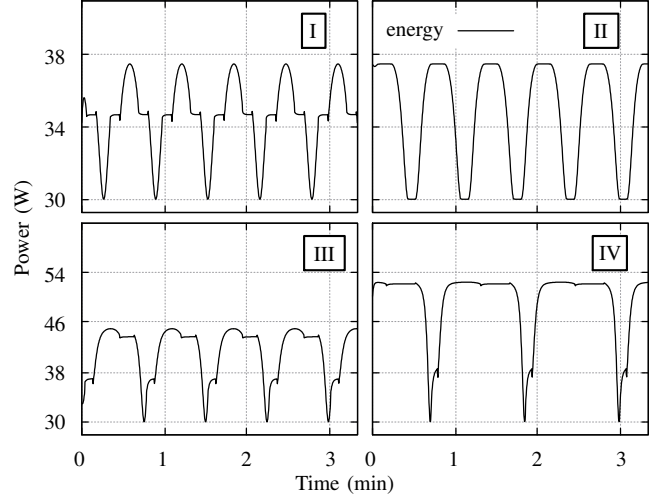
*

REFERENCES

- [1] P. Daponte, L. De Vito, L. Glielmo, L. Iannelli, D. Liuzza, F. Picariello, and G. Silano, "A review on the use of drones for precision agriculture," in *IOP Conference Series: Earth and Environmental Science*, vol. 275, no. 1. IOP Publishing, 2019, p. 012022.
- [2] Paparazzi. UAV open-source project. [Online]. Available: <http://wiki.paparazziuav.org/>
- [3] PX4. PX4 open-source autopilot. [Online]. Available: <https://px4.io/>
- [4] Y. Mei, Y.-H. Lu, Y. C. Hu, and C. G. Lee, "Energy-efficient motion planning for mobile robots," in *IEEE International Conference on Robotics and Automation, 2004. Proceedings. ICRA'04. 2004*, vol. 5. IEEE, 2004, pp. 4344–4349.
- [5] M. Wahab, F. Rios-Gutierrez, and A. El Shahat, *Energy modeling of differential drive robots*. IEEE, 2015.
- [6] C. H. Kim and B. K. Kim, "Energy-saving 3-step velocity control algorithm for battery-powered wheeled mobile robots," in *Proceedings of the 2005 IEEE international conference on robotics and automation*. IEEE, 2005, pp. 2375–2380.
- [7] H. Kim and B.-K. Kim, "Minimum-energy translational trajectory planning for battery-powered three-wheeled omnidirectional mobile robots," in *2008 10th International Conference on Control, Automation, Robotics and Vision*. IEEE, 2008, pp. 1730–1735.
- [8] Y. Mei, Y.-H. Lu, Y. C. Hu, and C. G. Lee, "A case study of mobile robot's energy consumption and conservation techniques," in *ICAR'05. Proceedings., 12th International Conference on Advanced Robotics, 2005*. IEEE, 2005, pp. 492–497.
- [9] S. T. H. Rizvi, G. Cabodi, D. Patti, and M. M. Gulzar, "A general-purpose graphics processing unit (ggpu)-accelerated robotic controller using a low power mobile platform," *Journal of Low Power Electronics and Applications*, vol. 7, no. 2, p. 10, 2017.
- [10] A. Abramov, K. Pauwels, J. Papon, F. Worgotter, and B. Dellen, "Real-time segmentation of stereo videos on a portable system with a mobile gpu," *IEEE Transactions on Circuits and Systems for Video Technology*, vol. 22, no. 9, pp. 1292–1305, 2012.
- [11] M. T. Satria, S. Gurumani, W. Zheng, K. P. Tee, A. Koh, P. Yu, K. Rupnow, and D. Chen, "Real-time system-level implementation of a telepresence robot using an embedded gpu platform," in *2016 Design, Automation & Test in Europe Conference & Exhibition (DATE)*. IEEE, 2016, pp. 1445–1448.
- [12] U. Jaramillo-Avila, J. M. Aitken, and S. R. Anderson, "Visual saliency with foveated images for fast object detection and recognition in mobile robots using low-power embedded gpus," in *2019 19th International Conference on Advanced Robotics (ICAR)*. IEEE, 2019, pp. 773–778.
- [13] Y. Mei, Y.-H. Lu, Y. C. Hu, and C. G. Lee, "Deployment of mobile robots with energy and timing constraints," *IEEE Transactions on robotics*, vol. 22, no. 3, pp. 507–522, 2006.
- [14] A. Sadrpour, J. Jin, and A. G. Ulsoy, "Mission energy prediction for unmanned ground vehicles using real-time measurements and prior knowledge," *Journal of Field Robotics*, vol. 30, no. 3, pp. 399–414, 2013.
- [15] —, "Experimental validation of mission energy prediction model for unmanned ground vehicles," in *2013 American Control Conference*. IEEE, 2013, pp. 5960–5965.
- [16] F. Morbidi, R. Cano, and D. Lara, "Minimum-energy path generation for a quadrotor uav," in *2016 IEEE International Conference on Robotics and Automation (ICRA)*. IEEE, 2016, pp. 1492–1498.
- [17] N. Kreciglowa, K. Karydis, and V. Kumar, "Energy efficiency of trajectory generation methods for stop-and-go aerial robot navigation," in *2017 International Conference on Unmanned Aircraft Systems (ICUAS)*. IEEE, 2017, pp. 656–662.
- [18] A. Seewald, U. P. Schultz, E. Ebeid, and H. S. Midtiby, "Coarse-grained computation-oriented energy modeling for heterogeneous parallel embedded systems," *International Journal of Parallel Programming*, pp. 1–22, 2019. [Online]. Available: <https://adamseew.bitbucket.io/short/coarse2019>
- [19] H. G. De Marina, Y. A. Kapitanuk, M. Bronz, G. Hattenberger, and M. Cao, "Guidance algorithm for smooth trajectory tracking of a fixed wing uav flying in wind flows," in *2017 IEEE international conference on robotics and automation (ICRA)*. IEEE, 2017, pp. 5740–5745.
- [20] S. R. Lindemann and S. M. LaValle, "Smoothly blending vector fields for global robot navigation," in *Proceedings of the 44th IEEE Conference on Decision and Control*. IEEE, 2005, pp. 3553–3559.
- [21] V. M. Gonçalves, L. C. Pimenta, C. A. Maia, B. C. Dutra, and G. A. Pereira, "Vector fields for robot navigation along time-varying curves in n -dimensions," *IEEE Transactions on Robotics*, vol. 26, no. 4, pp. 647–659, 2010.

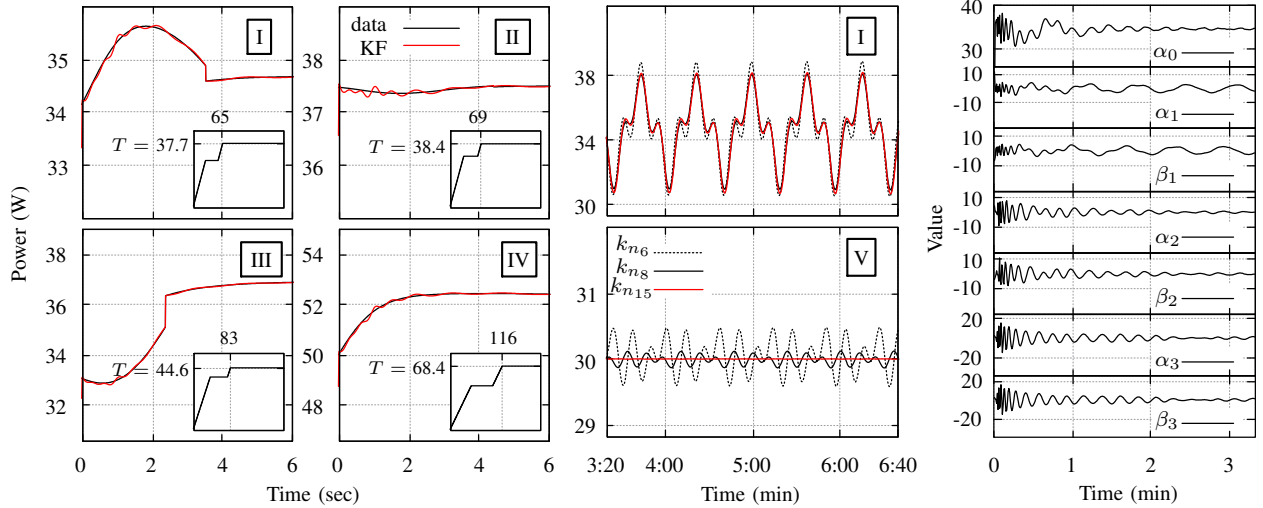


(a) path simulation, + is the UAV location after 200 seconds



(b) energy evolution simulation for 200 seconds interval

Fig. 5. Path and energy simulations with different atmospheric conditions. Simulations are performed from collected data by variations of wind speed and direction. The path and computations are static



(a) slice of the simulated energy along the estimated model

(b) model evolution at different k_s

(c) path I coefficients evolution

Fig. 6. Evolution of the simulated energy data from Figure 5, using the estimation first in a, the data with no estimation predicting the future in b, and evolution of the estimated coefficients in c

- [22] D. Panagou, "Motion planning and collision avoidance using navigation vector fields," in *2014 IEEE International Conference on Robotics and Automation (ICRA)*. IEEE, 2014, pp. 2513–2518.
- [23] D. Zhou and M. Schwager, "Vector field following for quadrotors using differential flatness," in *2014 IEEE International Conference on Robotics and Automation (ICRA)*. IEEE, 2014, pp. 6567–6572.
- [24] Y. A. Kapitanyuk, A. V. Proskurnikov, and M. Cao, "A guiding vector-field algorithm for path-following control of nonholonomic mobile robots," *IEEE Transactions on Control Systems Technology*, vol. 26, no. 4, pp. 1372–1385, 2017.
- [25] A. Seewald, H. Garcia de Marina, H. S. Midtiby, and U. P. Schultz, "Mechanical and computational energy estimation of a fixed-wing drone," in *2020 Fourth IEEE International Conference on Robotic Computing (IRC)*. IEEE, 2020, pp. 135–142. [Online]. Available: <https://adamseew.bitbucket.io/short/mechanical2020>
- [26] S. S. H. Hajjaj and K. S. M. Sahari, "Review of research in the area of agriculture mobile robots," in *The 8th International Conference on Robotic, Vision, Signal Processing & Power Applications*. Springer, 2014, pp. 107–117.
- [27] F. Qingchun, Z. Wengang, Q. Quan, J. Kai, and G. Rui, "Study on strawberry robotic harvesting system," in *2012 IEEE International Conference on Computer Science and Automation Engineering (CSAE)*, vol. 1. IEEE, 2012, pp. 320–324.
- [28] F. Dong, W. Heinemann, and R. Kasper, "Development of a row guidance system for an autonomous robot for white asparagus harvesting," *Computers and Electronics in Agriculture*, vol. 79, no. 2, pp. 216–225, 2011.
- [29] Z. De-An, L. Jidong, J. Wei, Z. Ying, and C. Yu, "Design and

- control of an apple harvesting robot,” *Biosystems engineering*, vol. 110, no. 2, pp. 112–122, 2011.
- [30] A. Aljanobi, S. Al-Hamed, and S. Al-Suhaibani, “A setup of mobile robotic unit for fruit harvesting,” in *19th International Workshop on Robotics in Alpe-Adria-Danube Region (RAAD 2010)*. IEEE, 2010, pp. 105–108.
 - [31] Z. Li, J. Liu, P. Li, and W. Li, “Analysis of workspace and kinematics for a tomato harvesting robot,” in *2008 International Conference on Intelligent Computation Technology and Automation (ICICTA)*, vol. 1. IEEE, 2008, pp. 823–827.
 - [32] Y. Edan, D. Rogozin, T. Flash, and G. E. Miles, “Robotic melon harvesting,” *IEEE Transactions on Robotics and Automation*, vol. 16, no. 6, pp. 831–835, 2000.
 - [33] V. Puri, A. Nayyar, and L. Raja, “Agriculture drones: A modern breakthrough in precision agriculture,” *Journal of Statistics and Management Systems*, vol. 20, no. 4, pp. 507–518, 2017.
 - [34] J. B. Rawlings, D. Q. Mayne, and M. Diehl, *Model predictive control: theory, computation, and design*. Nob Hill Publishing Madison, WI, 2017, vol. 2.
 - [35] A. Seewald, U. P. Schultz, J. Roeder, B. Rouxel, and C. Grelck, “Component-based computation-energy modeling for embedded systems,” in *Proceedings Companion of the 2019 ACM SIGPLAN International Conference on Systems, Programming, Languages, and Applications: Software for Humanity*. ACM, 2019, pp. 5–6. [Online]. Available: <https://adamseew.bitbucket.io/short/component2019>
 - [36] G. Zamanakos, A. Seewald, H. S. Midtiby, and U. P. Schultz, “Energy-aware design of vision-based autonomous tracking and landing of a uav,” in *2020 Fourth IEEE International Conference on Robotic Computing (IRC)*. IEEE, 2020, pp. 294–297. [Online]. Available: <https://adamseew.bitbucket.io/short/energy2020>
 - [37] D. Simon, *Optimal state estimation: Kalman, H infinity, and nonlinear approaches*. John Wiley & Sons, 2006.
 - [38] B. Kuo, *Automatic Control Systems*, ser. Electrical engineering series. Prentice-Hall, 1967.
 - [39] K. Ogata, *Modern Control Engineering*. Prentice Hall, 2002.
 - [40] C. Moler and C. Van Loan, “Nineteen dubious ways to compute the exponential of a matrix, twenty-five years later,” *SIAM review*, vol. 45, no. 1, pp. 3–49, 2003.

APPENDIX I
PROOF OF LEMMA III.1

We propose a formal proof of Lemma III.1. The proof justifies the choice of the items of the matrices A, C and of the initial guess \mathbf{q}_0 in Equation (3). We write these elements such that the coefficients of the series a_0, \dots, b_r are the same as the coefficients of the state α_0, \dots, β_r .

Let us re-write the Fourier series expression in Equation (1) in its complex form with the well-known Euler's formula $e^{it} = \cos t + i \sin t$. With $t = \omega j t$, we find the expression for $\cos \omega j t = (e^{i\omega j t} + e^{-i\omega j t})/2$ and $\sin \omega j t = (e^{i\omega j t} - e^{-i\omega j t})/(2i)$ by substitution of $\sin \omega j t$ and $\cos \omega j t$ respectively. This leads [38]

$$h(t) = a_0/T + (1/T) \sum_{j=1}^r e^{i\omega j t} (a_j - ib_j) + (1/T) \sum_{j=1}^r e^{-i\omega j t} (a_j + ib_j), \quad (9)$$

where i is the imaginary unit.

The solution at time t can be expressed $\mathbf{q} = e^{At} \mathbf{q}_0$. Both the solution and the system in Equation (2) are well established expressions derived using standard textbooks [38], [39]. To solve the matrix exponential e^{At} , we use the eigenvectors matrix decomposition method [40].

The method works on the similarity transformation $A = VDV^{-1}$. The power series definition of e^{At} implies $e^{At} = Ve^{Dt}V^{-1}$ [40]. We consider the non-singular matrix V , whose columns are eigenvectors of A ; $V := [v_0 \ v_1^0 \ v_1^1 \ \dots \ v_r^0 \ v_r^1]$. We then consider the diagonal matrix of eigenvalues $D = \text{diag}(\lambda_0, \lambda_1^0, \lambda_1^1, \dots, \lambda_r^0, \lambda_r^1)$. λ_0 is the eigenvalue associated to the first item of A . λ_j^0, λ_j^1 are the two eigenvalues associated with the block A_j . We can write $Av_j = \lambda_j v_j \ \forall j = \{1, \dots, m\}$, and $AV = VD$.

We apply the approach in terms of Equation (2), under the assumptions made in the lemma (the control is a zero vector); $\dot{\mathbf{q}} = A\mathbf{q}$. The linear combination of the initial guess and the generic solution

$$F\mathbf{q}(0) = \gamma_0 v_0 + \sum_{k=0}^1 \sum_{j=1}^r \gamma_j v_j^k \quad (10)$$

$$F\mathbf{q}(t) = \gamma_0 e^{\lambda_0 t} v_0 + \sum_{k=0}^1 \sum_{j=1}^r \gamma_j e^{\lambda_j^k t} v_j^k$$

where $F = [1 \ \dots \ 1]$ is a properly sized vector of ones.

We proof that the eigenvalues λ and eigenvectors V are such that Equation (11) is equivalent to Equation (9).

Let us consider the second expression in Equation (10). It represents the linear combination of all the coefficients of the state at time t . It can also be expressed

in the following form

$$F\mathbf{q}(t)/T = \gamma_0 e^{\lambda_0 t} v_0/T + (1/T) \sum_{j=1}^r \gamma_j e^{\lambda_j^0 t} v_j^0 + (1/T) \sum_{j=1}^r \gamma_j e^{\lambda_j^1 t} v_j^1. \quad (11)$$

The matrix A is a block diagonal matrix, so we can express its determinant as the multiplication of the determinants of its blocks $\det(A) = \det(0) \times \det(A_1) \times \dots \times \det(A_r)$. We proof the first determinant and the others separately.

Thereby we start by proofing that the first terms of the Equation (9) and (11) match. We find the eigenvalue from $\det(0) = 0$, which is $\lambda_0 = 0$. The corresponding eigenvector can be chosen arbitrarily ($0 - \lambda_0)v_0 = [0 \ \dots \ 0] \ \forall v_0$, thus we choose $v_0 = [1 \ 0 \ \dots \ 0]$. We find the value γ_0 of the vector γ so that the terms are equal, $\gamma_0 = [a_0 \ 0 \ \dots \ 0]$.

Then, we proof that all the terms in the sum of both the Equations (9) and (11) match.

For the first block A_1 , we find the eigenvalues from $\det(A_1 - \lambda I) = 0$. The polynomial $\lambda^2 + \omega^2$, gives two complex roots—the two eigenvalues $\lambda_1^0 = i\omega$ and $\lambda_1^1 = -i\omega$. The eigenvector associated with the eigenvalue λ_1^0 is $v_1^0 = [0 \ -i \ 1 \ 0 \ \dots \ 0]^T$. The eigenvector associated with the eigenvalue λ_1^1 is $v_1^1 = [0 \ i \ 1 \ 0 \ \dots \ 0]^T$. Again, we find the values γ_1 of the vector γ such that the equivalences

$$\begin{cases} e^{i\omega t} (a_1 - ib_1) &= \gamma_1 e^{i\omega t} v_1^0 \\ e^{-i\omega t} (a_1 + ib_1) &= \gamma_1 e^{i\omega t} v_1^1 \end{cases}$$

hold. They hold for $\gamma_1 = [b_1 \ a_1]$.

The proof for the remaining $r-1$ blocks is equivalent.

The initial guess is build such that the sum of the coefficients is the same in both the signals. In the output matrix, the frequency $1/T$ accounts for the period in Equation (9) and (11) and (1). At time instant zero, the coefficients b_j are not present and the coefficients a_j are doubled for each $j = 1, 2, \dots, r$ (thus we multiply by a half the corresponding coefficients in \mathbf{q}_0). To match the outputs $h(t) = y(t)$ —or equivalently $F\mathbf{q}(t)/T = C\mathbf{q}(t)$ —we define $C = (1/T) [1 \ 1 \ 0 \ \dots \ 1 \ 0]$. We thus conclude that the signal and the output are equal, hence the lemma holds. ■

We note for practical reasons that the signal would still be periodic with another linear combination of coefficients (for instance, $C = d [1 \ 0 \ 1 \ \dots \ 0 \ 1]$, or $d [1 \ \dots \ 1]$ for a constant value $d \in \mathbb{R}$).